CRYSTALLINITY EFFECTS ON VIS-NIR FEATURES OF SAPONITE: IMPLICATIONS FOR CHARACTERIZING VARIABLE CRYSTALLINE PHYLLOSILICATES ON MARS. Lingxi Zhang[1], Xiaohui Fu[1*], Alian Wang[2], Zongcheng Ling[1] [1] Shandong Provincial Key Laboratory of Optical Astronomy and Solar-Terrestrial Environment, Institute of Space Sciences, Shandong University, Weihai, China. (fuxh@sdu.edu.cn), [2] Department of Earth and Planetary Sciences and The McDonnell Center for the Space Sciences and McDonnell Center for Space Sciences, Washington University, St. Louis, MO, USA.

Introduction: Phyllosilicates as the key indicators of past aqueous activity, are important for understanding the hydrologic history of Mars [1]. VIS-NIR spectral observations obtained by the CRISM and the OMEGA spectrometer have detected spectral signatures at numerous locations across the Martian surface indicating the presence of clay minerals [1-4]. These identifications are mainly based on the detection of H_2O combinations at 1.9 μm, overtones of O-H stretching in both OH groups and adsorbed water at 1.4 μm, and Metal-OH combination band at 2.2-2.4 μm. In-situ mineralogical characterization by CheMin revealed the poorly crystalline smectite in Gale crater, indicating that martian clays have complex structure feature and formation process [5].

The identification and characterization of phyllosilicates on Mars on a global scale will continue to rely on VIS-NIR spectroscopic orbital remote sensing [6]. Current orbital methods depend on matching measured spectral features with those in a mineral spectral library. However, there are no data of poorly crystalline phyllosilicates in the VIS-NIR spectral libraries.

In this study, we focus on a Mg-endmember of smectite (saponite) with different degrees of crystallinity, investigate the difference of vibrational spectroscopy among the variable crystalline phyllosilicate, and evaluate the utility of using the spectral features for general Mars mission data interpretation.

Materials and Methods: The saponite was synthesized using a sol-gel method. A buffer solution of pH=11 was prepared by dissolving NaOH and $NaHCO_3$ in deionized water. Then, sodium metasilicate powder was added to 25 mL of the buffer solution under vigorous stirring. A second solution was prepared by dissolving aluminum chloride and magnesium chloride in 25 mL of deionized water. The second solution was entirely added into the buffer solution with an eyedropper under magnetic stirring at room temperature. The mixed solution was then transferred into a Teflon beaker, sealed, and heated in an incubator at different temperatures (80-200 ºC) for 24 h. After the hydrothermal process, the products were rinsed 3 times with deionized water by centrifugation. The obtained precipitations were then dried in a 50 ºC oven for 24 h. The obtained products were marked as Sap-X (X=synthesis temperature) in the present study.

XRD was used to characterize the products' phase and VIS-NIR spectroscopy was carried to obtained the structural difference between the variable crystallized saponites.

Results: The XRD result confirm that the products are all saponite. And their crystallinity increases with the rising synthesis temperature, indicated by the width of 060 peak,

The NIR spectra of synthetic saponite (Fig. 1) exhibit strong and broad water overtone near 1.41 μm with a sharp peak at 1.39 μm due to the overtones of the OH stretching band. The combination of the stretching plus bending vibration modes of water appears at 1.91 μm [2]. The multipeak band in the spectral region from 2.20 to 2.40 μm is contributed by the combination of in-plan bending of Metal-OH and the stretching mode of OH [7]. The OH combination bands occur near 2.2 μm are due to coordinated Al cations in octahedral sites, while OH stretching and bending combination bands occur near 2.29 μm and 2.32 μm is related to coordinated Fe and Mg cations in octahedral sites [8].

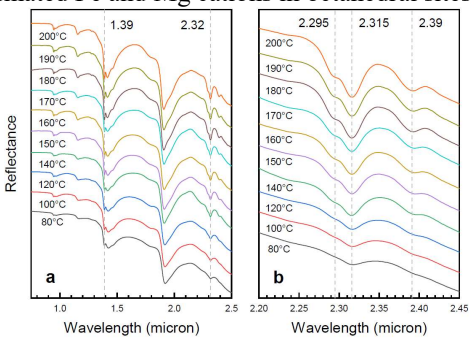

Fig. 1 VIS-NIR spectra of synthetic saponite samples. (a) The reflectance spectra of saponite samples in the 0.35-2.5 μm range. (b) The multipeak band (Metal-OH) in the NIR 2.2-2.4 μm of saponite samples.

Following the increasing crystallinity of synthetic saponite, the spectral resolution of the band at 2.20-2.40 μm increases. To quantify the effect of crystallinity changes on spectral resolution for the diagnostic Metal-OH absorptions for saponite, we calculated the first derivative of the spectra, and use the morphologic changes of the first derivatives of the diagnostic Metal-OH doublets as a crystallinity index (Fig. 2). The first derivative of reflectance at 2.297 μm increase with the rising degree of crystallinity as well as the synthesis temperature (Fig. 2b). This observation implies the

increasing ordering of the Mg^{2+} (Al^{3+}) arrangement in octahedral sheets. In general sense, the first derivative of reflectance of Metal-OH doublets could be used to detect changes in crystallinity of saponite.

Discussion: In order to verify the usability of the first derivatives of reflectance, we resampled the NIR spectra of synthetic saponite to a wavelength resolution of 6.55 nm using ENVI 5.3 software (Fig 3). It was found that the decreased spectral resolution didn't change the diagnostic features of saponite and the similar patterns of Metal-OH doublets was noted in the derivatived reflectance spectra.

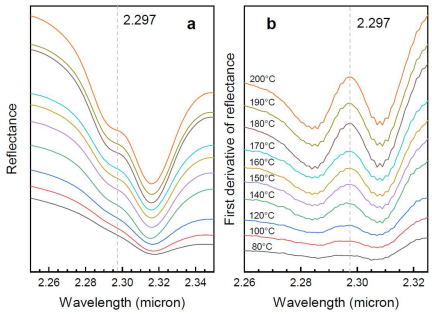

Fig. 2 NIR spectra of the diagnostic doublets and their derivatives. (a) NIR spectra of the diagnostic doublets of Metal-OH band. (b) The first derivative of the diagnostic peaks.

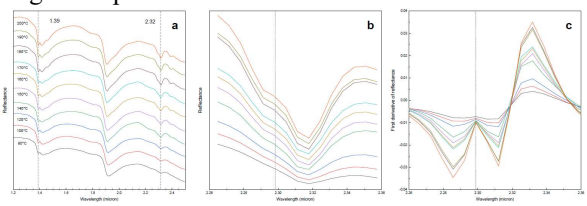

Fig. 3 Resampled NIR spectra and their first derivatives of synthetic saponites in this study. (a) The resampled reflectance spectra of saponite samples in the 0.35-2.5 μm range. (b) The resampled spectra of the diagnostic doublets of Metal-OH band. (c) The first derivatives of resampled spectra of the diagnostic doublets.

We also obtained CRISM spectra of Mg-smectite from Nili Fossae (21.1522 °N, 74.2491 °E, FRT000064-D9) (Fig. 4). According to our interpretation of the first derivative of the Metal-OH doublets based on lab data, the CRISM spectra were divided into two categories (Fig. 5). Type A (Fig. 5a) represents spectra with well-resolved doublets at 2.20-2.40 μm, and type B (Fig. 5c) are characterized by only one broad peak in the spectra. The first derivatives of type A (Fig. 5b) at 2.306 μm all exhibit an upward angle. This is caused by the good degree of separation between the two peaks. And the first derivatives of type B (Fig. 5d) at 2.306 μm only show a single tend slope, which is due to the low spectral resolution.

Comparing the resampled NIR reflectance spectra of the synthetic saponite from this study with the CRISM spectra, the first derivative of type A matches to the saponite synthesized at higher temperatures (200 ºC to 140 ºC), while the derivative of type B matches to the lower ones. Thus, type A delegates saponite with good crystallinity, and type B refers to poorly crystallized saponite. This result validates our suggestion of using the first derivative of the Metal-OH band in the NIR range to infer the structural ordering of martian smectite on a global scale. The structural information for smectite could help us better understand their formation conditions (e.g., temperature, duration, and pH values) [9] and the conditions of hydrothermal aqueous alteration on Mars.

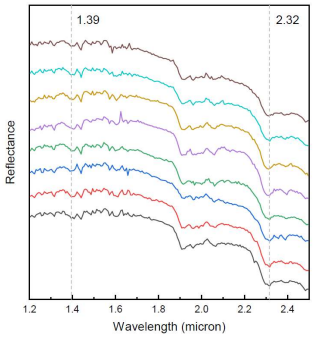

Fig.4 CRISM spectra obtained from FRT000064D9.

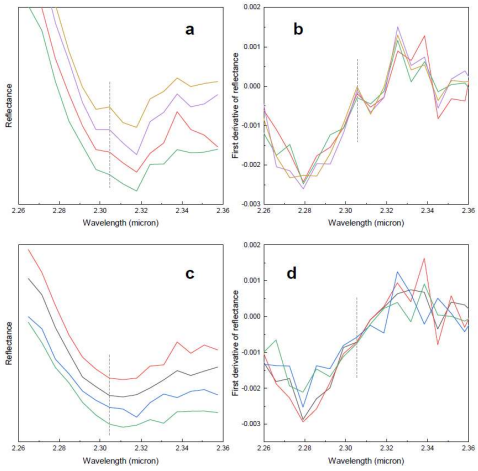

Fig. 5 Two types (type A and type B) of CRISM spectra and their derivatives. (a, c) Two types of CRISM spectra. (b, d) The first derivatives of (a) and (c).

References: [1] Bibring, J.P. et al. (2006) Science, 312(5772), 400–404. [2] Bishop, J.L. et al. (2008) Clay Minerals, 43, 35–54. [3] Mustard, J.F. et al. (2008) Nature, 454, 305–309. [4] Poulet, F. et al. (2005) Nature, 438(7068), 623–627. [5] Vaniman, D. et al. (2014) Science, 343, 1243480. [6] Cuadros, J. et al. (2016) American Mineralogist, 101, 554–563. [7] Bishop, J.L. et al. (2002) Clay Minerals, 37, 607–616. [8] Carter, J. et al. (2013) Journal of Geophysical Research: Planets, 118, 831–858. [9] Petit, S. et al. (2015) Applied Clay Science, 104, 96–105.